Korean J. Chem. Eng., **25**(6), 1292-1299 (2008)

Effect of fluid velocity and temperature on the corrosion mechanism of low carbon steel in industrial water in the absence and presence of 2-hydrazino benzothiazole

Aswaidy Mohammed Badiea† and Kikkeri Narasimhasetty Mohana

Department of Studies in Chemistry, University of Mysore, Manasagangotri, Mysore-570 006, India
(*Received 14 February 2008 • accepted 18 March 2008*)

Abstract–This work was carried out to study the inhibition mechanism of volatile corrosion inhibitors (VCIs) such as 2-hydrazinobenzothiazole (2-HBTA) on the corrosion of low carbon steel in industrial water by using polarization and mass loss measurement. It was found that 2-HBTA revealed good performance as inhibitor for low carbon steel corrosion in industrial water. After some time, the performance decreased due to the volatility of these kinds of inhibitors away from the open system unlike the closed system. The experimental data indicated that the inhibitive performance of 2-HBTA for low carbon steel was improved with increasing of concentration up to the critical concentration (4.24×10^{-3} M). The adsorption behavior of 2-HBTA was found to obey Langmuir's adsorption isotherm. The thermodynamic parameters of adsorption process and activation energy were obtained from polarization technique. Scanning electron microscopy (SEM) was performed to characterize the film formed on the surface. Box-Wilson statistical method was employed to correlate the results obtained, and the optimization of fluid velocity, temperature and concentration of inhibitor by using Box-Wilson statistical method was evaluated.

Key words: Metals and Alloys, Surfaces and Interfaces, Corrosion, SEM

INTRODUCTION

Volatile corrosion inhibitors (VCIs) are compounds that have the ability to vaporize and condense on a metallic surface to make it less susceptible to corrosion. The main advantage of VCIs compared with conventional corrosion control methods stems from their gas-phase transport, which enables them to reach all metallic surfaces without actually having to bring the solid VCIs into direct contact with surface.

The inhibition mechanism of VCIs depends mainly on how the inhibitors pass into the vapor state and how they subsequently protect the metallic surface [1]. In heat exchangers, all types of water used for cooling or heating the products contain very high chloride concentrations and other anions of metals and biocarbonates. Therefore, the injection of a corrosion inhibitor through different sites of pipes is very important. The inhibition of mild steel corrosion in aqueous solution by organic [2-4] and inorganic [5,6] compounds was extensively studied. Most of the efficient inhibitors used in industry are organic compounds having multiple bonds in their molecules [7] which contain nitrogen and sulfur atoms that are adsorbed on the metal surface. It is well known that the application of VICs is one of the most practical methods for the protection of metals against atmospheric corrosion [8].

The advantage of VCIs is that the vaporized inhibitive molecules can reach hard-to-reach areas at room temperature and form a relatively stable layer on the metal surface. The protective layer of VCIs will not interfere because this layer is very thin [9]. Solids VCIs such as salts of dicyclohexylamine, cyclohexaylamine and hexamethylene-amine on contact with the metal surface can inhibit the carbon steel corrosion. However, the application of those inhibitors has been confined due to their toxicity. The vapor of these salts condenses and is hydrolyzed by any moisture to liberate protective ions [10]. In the present investigation the use of 2-HBTA as volatile corrosion inhibitor (VCI) for low carbon steel in industrial water was studied as a friendly corrosion inhibitor. The VCIs are transported with steam to prevent steel corrosion in condenser tubes by neutralizing acidic carbon dioxide or by shifting surface pH value towards the less acidic [10]. The selection of the suitable inhibitors mainly depends on the type of industrial environment, type of ions it contains, velocity of the fluid, and environment temperature.

Thermodynamic parameters such as adsorption heat, adsorption entropy, adsorption enthalpy and adsorption Gibbs free energy were obtained from experimental data of the inhibition process at different temperatures. The apparent activation energy and pre-exponential factor at different concentration of inhibitor were also calculated and their effects on the corrosion rate of low carbon steel were discussed.

EXPERIMENTAL WORK

1. Materials Preparation

The corrosion tests were performed on low carbon steel coupons cut from pipe which had the following composition (wt %): 0.15- C; 0.37- Si; 0.04- P; 0.01- Al; 0.05- Mn; 0.05- S and the remainder iron. The test solution used was industrial water coming from heat exchangers and reboilers of chemical industries around Mysore city. The pH of the industrial water was 6.9 and the chemical compositions (ppm) using ionic chromatograph were analyzed and given as the following: 65122 Cl^-; 950 Ca^{+2}; 650 SO_4^{2-}; 450 Mg^{2+}; 64 HCO_3^-; 18657 Na^+. The structure of 2-HBTA selected after studying four compounds is shown in Fig. 1. For the gravimetric and potentiodynamic measurements, some treatment for the surface of specimens was carried out. Prior to each experiment, the

†To whom correspondence should be addressed.
E-mail: badeea7@yahoo.com

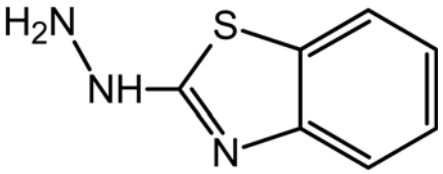

2-HBTA

Fig. 1. Chemical structure of 2-HBTA.

surface of the specimen was polished under running tap water by using emery paper of grade numbers 220, 320, 450, and 600, rinsed with distilled water, dried on a clean tissue paper, immersed in benzene for five seconds, dried and immersed in acetone for five seconds and dried with clean tissue paper. Finally, they were kept in a desiccator for one hour until use.

2. Mass Loss Measurements

The initial weight of the specimen was recorded by using an analytical balance (precision ±0.1 mg) before immersion in industrial water. The corrosion rates of low carbon steel were determined for 10 hrs of immersion period at various rotational speeds (1,500-2,100 rpm) from mass loss by using Eq. (1), where W is the mass loss (g), t is the immersion time (hrs), and A is the area of the cylinder coupon (mm^2). The corrosion rate (CR) is expressed in g m^{-2} d^{-1} or gmd.

$$CR = \frac{24 \times 10^6 W}{t \cdot A} \tag{1}$$

The inhibition efficiency (IE %) and surface coverage degree (θ) were obtained as the following:

$$IE(\%) = \frac{CR_a - CR_p}{CR_a} \times 100 \tag{2}$$

$$\theta = \frac{CR_a - CR_p}{CR_a} \tag{3}$$

Where CR_a and CR_p are the corrosion rate in absence and presence of inhibitor, respectively. The temperature of the environment was maintained by thermostatically controlled water bath (Eltek Ltd. Mumbai, India). The velocity of the specimens was set at a desired speed by using a speed regulator motor (Weiber Ltd. Chennai, India).

3. Electrochemical Polarization Measurements

Electrochemical measurements were done by means of potentiostat regulation with a Solartron 1286 electrochemical interface. The polarization curves were obtained for various temperatures and various electrode velocities. Every plotted point was scanned from −700 to 500 mV with a scan rate of 0.42 mV s^{-1} to ensure the steady-state condition.

Electrochemical experiments were carried out using a three-electrode glass cell with platinum and saturated calomel electrode (SCE) as a counter and reference electrode, respectively. All results were obtained from at least three experiments to ensure reproducibility. The protection efficiency and surface coverage degree can be also calculated from the electrochemical measurements as the following equations:

$$IE(\%) = \frac{I_{corr(a)} - I_{corr(p)}}{I_{corr(a)}} \times 100 \tag{4}$$

$$\theta = \frac{I_{corr(a)} - I_{corr(p)}}{I_{corr(a)}} \tag{5}$$

Where $I_{corr(a)}$ and $I_{corr(p)}$ are the corrosion current density in absence and presence of inhibitors, respectively, obtained by extrapolation of anodic and cathodic Tafel slopes to the corrosion potential. The corrosion rate (CR) can be also calculated from electrochemical measurements as the following:

$$CR = 8.954 \times 10^{-3} I_{corr} \times EW \tag{6}$$

Where I_{corr} is the corrosion current density (μA cm^{-2}), EW is the equivalent weight of low carbon steel (g) and CR is expressed in g m^{-2} d^{-1}. The method and the experimental setup have been presented in detail elsewhere [11].

RESULTS AND DISCUSSION

1. Mass Loss Measurements

Values of corrosion rate (CR), inhibition efficiency (IE %) and degree of surface coverage (θ) obtained from mass loss measurements of low carbon steel at 55 °C and different concentrations of inhibitor in industrial water at 1.44 and 1.56 m s^{-1} after 10 hrs of immersion are depicted in Table 1. Table 1 shows that the θ and IE increased with increasing the inhibitor concentration. The optimum concentration of 2-HBTA that was found to perform the highest efficiency was 4.2×10^{-3} M with the inhibitor efficiency of 78.08% at 55 °C and at 1.56 m s^{-1}. Although the presence of benzene ring, nitrogen and sulfur atoms in 2-HBTA, the IE (%) of 2-HBTA is relatively less than that of sodium diphenylamine-4-sulfate (SDPAS) (our previous study). This is because the 2-HBTA is a volatile corrosion inhibitor since it is very sensitive to temperature and the other conditions, and also the SDPAS is more adherently adsorbed than 2-HBTA on low carbon steel surface due to its high electronegativity. This consideration is enhanced by the high negative values of ΔS_a for SDPAS (ΔS_a=−209.94 J mol^{-1} K^{-1} at optimum conditions), whereas ΔS_a for 2-HBTA was −182.82 J mol^{-1} K^{-1} at optimum conditions. These compounds can be also adsorbed on the metal surface by the interaction between lone pairs of electrons of nitrogen and sulfur atoms and metal surface. This process is facilitated by the presence of vacant orbital of low energy in iron atom, as observed in the transition group metals [12].

2. Electrochemical Polarization

Table 1. CR, IE (%) and θ obtained from weight loss measurements of low carbon steel in industrial water containing various concentrations of 2-HBTA at 55 °C and at 1.44 and 1.56 m s^{-1}

C (M)	1.44 m s^{-1}			1.56 m s^{-1}		
	CR (g m^{-2} d^{-1})	IE (%)	θ	CR (g m^{-2} d^{-1})	IE (%)	θ
blank	10.35			12.06		
6.1×10^{-4}	6.25	39.64	0.396	7.23	40.08	0.401
1.2×10^{-3}	5.48	47.11	0.471	5.82	51.78	0.518
2.4×10^{-3}	4.72	54.42	0.544	4.83	59.93	0.599
3.6×10^{-3}	3.72	64.06	0.641	3.96	67.18	0.672
4.2×10^{-3}	2.65	74.38	0.744	2.64	78.08	0.7808

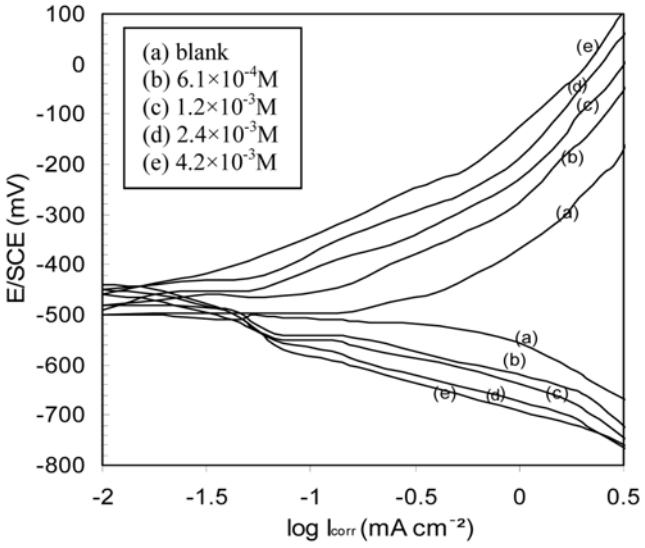

Fig. 2. Polarization curves for low carbon steel in industrial water containing different concentrations of 2-HBTA at 1.44 m s^{-1} and 55 °C (scan rate=0.42 mV s^{-1}).

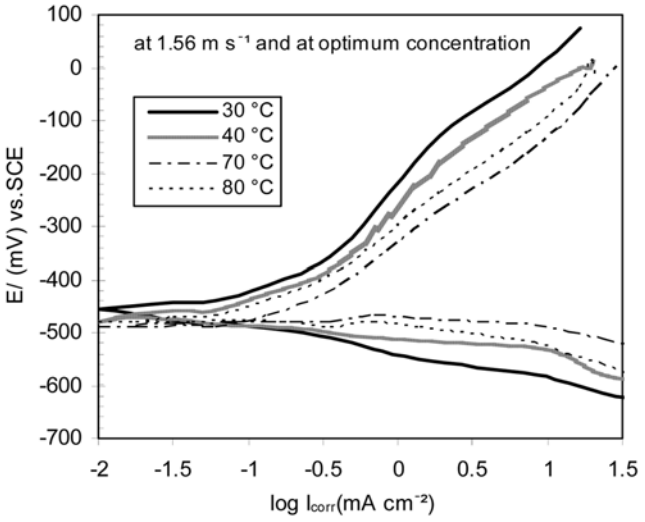

Fig. 3. Polarization curves of low carbon steel in industrial water at optimum concentration of 2-HBTA at different temperature (scan rate=0.42 mV s^{-1}).

The anodic and cathodic polarization curves of low carbon steel electrode in industrial water in absence and presence of different concentrations of 2-HBTA are shown in Fig. 2. For the anodic and cathodic branches interaction, the inhibitor shifts the anodic and cathodic lines to lower current densities. This implies that 2-HBTA acts as a mixed inhibitor. The curves of anodic and cathodic currents were inhibited with increasing of 2-HBTA concentrations, but anode curves reveal more of an effect. This means the addition of 2-HBTA reduces anodic dissolution and also retards the hydrogen evolution reaction at the cathodic. Table 2 presents the values of polarization parameters as the corrosion potential ($E_{corr.}$), corrosion current density ($I_{corr.}$) and IE (%) for the corrosion of low carbon steel in industrial water at different temperatures and at different concentrations of 2-HBTA. From Table 2, slight changes in the corrosion potential occur by the addition of inhibitor. Also there is a small shifting in E_{corr} towards the positive direction at 1.56 m s^{-1}. This indicates that the absorbed molecules of the inhibitor do not affect the mechanism of hydrogen evolution [13].

3. Effect of Temperature

To get good information on the mechanism of 2-HBTA on low carbon steel and to evaluate the activation energy and pre-expo-

Table 2. E_{corr}, I_{corr} and IE (%) obtained from electrochemical measurements for low carbon steel in industrial water containing various concentrations of 2-HBTA at different temperatures and at 1.44 and 1.56 m s^{-1}

T (°C)	C (M)	1.44 m s^{-1}			1.56 m s^{-1}		
		E_{corr} vs. SCE (mV)	I_{corr} (μA cm^{-2})	IE (%)	E_{corr} vs. SCE (mV)	I_{corr} (μA cm^{-2})	IE (%)
30	blank	−501	62.50		−508	80.35	
	6.1×10^{-4}	−498	36.05	42.32	−497	46.16	42.55
	1.2×10^{-3}	−498	30.99	50.41	−494	38.85	51.65
	2.4×10^{-3}	−490	25.76	58.79	−490	32.02	60.15
	3.6×10^{-3}	−489	19.48	68.83	−490	25.35	68.45
	4.2×10^{-3}	−489	16.59	73.45	−478	19.74	75.43
40	blank	−500	78.65		−511	112.3	
	6.1×10^{-4}	−499	45.18	42.55	−499	63.84	43.15
	1.2×10^{-3}	−492	38.37	51.22	−488	52.24	53.48
	2.4×10^{-3}	−492	31.12	60.43	−487	43.27	61.47
	3.6×10^{-3}	−485	26.84	65.88	−483	38.75	65.49
	4.2×10^{-3}	−483	17.35	77.94	−477	24.19	78.46
55	blank	−505	114.93		−513	155.43	
	6.1×10^{-4}	−499	69.08	39.89	−497	91.00	41.45
	1.2×10^{-3}	−491	55.30	51.88	−486	70.78	54.46
	2.4×10^{-3}	−501	44.31	61.45	−486	60.34	61.18
	3.6×10^{-3}	−488	37.41	67.45	−485	49.91	67.89
	4.2×10^{-3}	−485	26.23	77.18	−480	30.39	80.45

nential factor of the corrosion process, electrochemical measurements were taken at various temperature in the absence and in presence of different concentrations of the inhibitor. From Table 2 and Fig. 3, it is shown that the I_{corr} increases with increasing temperature in the presence and absence of 2-HBTA except at 80 °C. The decrease of I_{corr} at 80 °C is attributed to the escape of oxygen from the open system unlike the closed system. However, the I_{corr} decreased with increasing concentration of inhibitor. The IE (%) and θ also are nearly constant; this means they were temperature independent.

The activation energy for low carbon steel corrosion process was calculated by using the Arrhenius mode as the following equation:

$$I_{corr.} = k \cdot \exp\left(\frac{-E_a}{RT}\right) \tag{7}$$

And also the activation entropy and enthalpy were calculated from the alternative Arrhenius mode as the following equation:

$$I_{corr.} = \frac{RT}{hN}\exp\left(\frac{\Delta S_a}{R}\right)\cdot\left(\frac{-\Delta H}{RT}\right) \tag{8}$$

Where E_a is the apparent activation energy, k is the pre-exponential factor, R is the universal gas constant, T is the absolute temperature, h is Planck's constant, N is Avogadro's number, ΔH_a and ΔS_a are the enthalpy and entropy of activation, respectively. Plots of log I_{corr} and log (I_{corr}/T) versus 1/T gave slopes of ($-E_a$/2.303R) and ($-\Delta H_a$/2.303R) and intercepts of (log k) and [log (R/hN)+ΔS_a/2.303R)] as shown in Figs. 4 and 5, respectively. The summarized values of the above parameters are given in Table 3. It is shown that the values of E_a in the presence of 2-HBTA are lower than those in its absence. This may be attributed to the change of mechanism of inhibitor on metal surface leading to lower rate for dissolution of metal in solution. From Eq. (7), typically the higher in E_a and lower in k lead to a decrease in I_{corr}. However, in the present work the decrease in I_{corr} is mostly decided by the decrease of k [12]. Furthermore, the values of ΔH_a obtained are in good agreement with those obtained from Eq. (6) (Table 3).

$$\Delta H_a = E_a - RT \tag{9}$$

4. Effect of Velocity

As the fluid flows through the pipe, the rotational speed of the specimen is converted into the flow rate of the fluid by using the following empirical equations [14]:

$$q = 0.92 n D_a^3\left(\frac{D_t}{D_a}\right) \tag{10}$$

$$A_p = \pi D_a W \tag{11}$$

Where q is the total flow rate from the edges of impeller ($m^3\ s^{-1}$), n is the number of rotations per second, D_a is the impeller diameter (m), D_t is the diameter of solution vessel (m), A_p is the area of the cylinder swept out by the tips of the impeller blades (m^2), and W is the width of the impeller (m). The velocity of the fluid can be obtained by dividing Eq. (10) by Eq. (11). Fig. 6 shows that in the absence and presence of inhibitor, the corrosion current density, I_{corr}, increases with increasing velocity; and the inhibition efficiency was a maximum at 1.56 m s^{-1}. This is because a reasonable velocity is

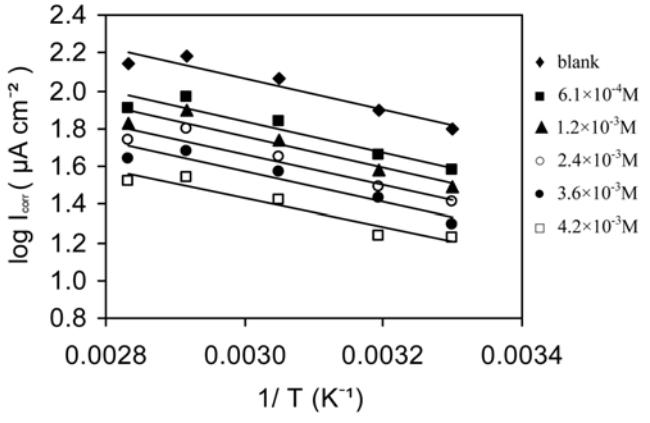

Fig. 4. Arrhenius plots for low carbon steel dissolution in industrial water in absence and presence of different concentrations of 2-HBTA at 1.44 m s^{-1}.

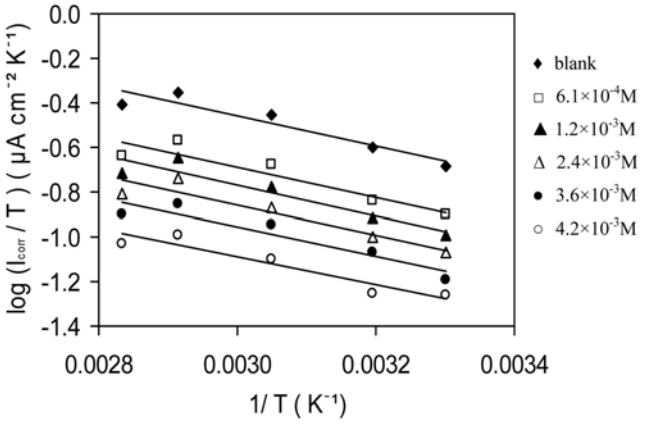

Fig. 5. Alternative Arrhenius for low carbon steel dissolution in industrial water in absence and presence of different concentrations of 2-HBTA at 1.44 m s^{-1}.

Table 3. Values of activation parameters for low carbon steel in industrial water in absence and presence of different concentrations of 2-HBTA at 1.44 m s^{-1}

C (M)	k (μA cm^{-2})	E_a (kJ mol^{-1})	ΔH_a (kJ mol^{-1})	$\Delta H_a = E_a - RT$ (kJ mol^{-1})	ΔS_a (J mol^{-1} K^{-1})
blank	33,760.00	15.74	13.02	13.22	−167.36
6.1×10^{-4}	19,085.34	15.60	12.88	13.08	−172.10
1.2×10^{-3}	17,930.81	15.64	13.22	13.42	−172.62
2.4×10^{-3}	12,664.85	15.56	12.84	13.04	−175.51
3.6×10^{-3}	9,576.35	15.39	12.68	12.87	−177.84
4.2×10^{-3}	5,262.60	14.60	11.89	12.09	−182.82

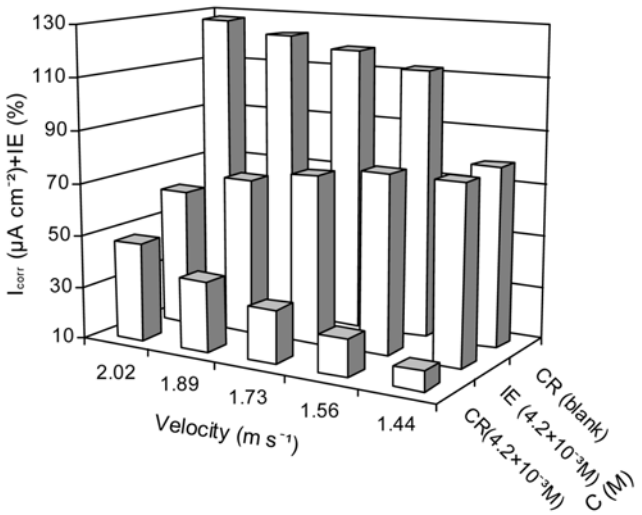

Fig. 6. Effect of fluid velocity on IE (%) and corrosion current density in presence and absence of 2-HBTA on low carbon steel in industrial water at optimum concentration and at 40 °C.

necessary to distribute the inhibitor properly and keep the suspended particles from precipitating on the metal surface, forming products which cause a pitting corrosion or erosion due to the flow. Beyond 1.56 m s^{-1}, the inhibition efficiency began decreasing because the greater the velocity, the thinner the laminar layer along the metal surface [15], so oxygen easily reaches the metal surface and causes more corrosion. Also, the presence of small suspended particles of dust, sand, etc., in solution acts by breaking the film formed on the metal surface and moves it away from the surface.

5. Adsorption Isotherm

To get more information regarding the mode of adsorption of 2-HBTA on low carbon steel surface, the experimental data were examined with several adsorption isotherms. The surface coverage degree (θ) of the inhibitor from electrochemical measurements was calculated from Eq. (5).

Many attempts were made to find the best isotherm that describes this study. The Langmuir adsorption isotherm was found to be the best one. According to this isotherm, θ is related to the inhibitor concentration, C, and equilibrium constant of adsorption process, K, via [16]:

$$\frac{\theta}{1-\theta} = KC \tag{12}$$

Rearranging this equation gives,

$$\frac{C}{\theta} = \frac{1}{K} + C \tag{13}$$

The plots of (C/θ) versus C give a straight line as shown in Fig. 7. The linear regression coefficients (R^2) are almost equal 0.989 and the slopes are very close to 1, confirming that the adsorption of 2-HBTA on the low carbon steel surface in industrial water obeys the Langmuir adsorption isotherm. The constant of adsorption (K) is related to the standard Gibbs free energy of adsorption, ΔG_{ads}:

$$K = \frac{1}{55.5}\exp\left(\frac{-\Delta G_{ads}}{RT}\right) \tag{14}$$

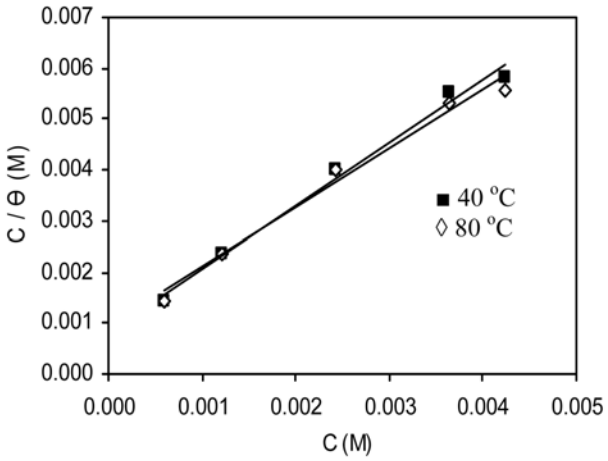

Fig. 7. Langmuir adsorption isotherm model for low carbon steel surface in industrial water at different temperature and at 1.44 m s^{-1}.

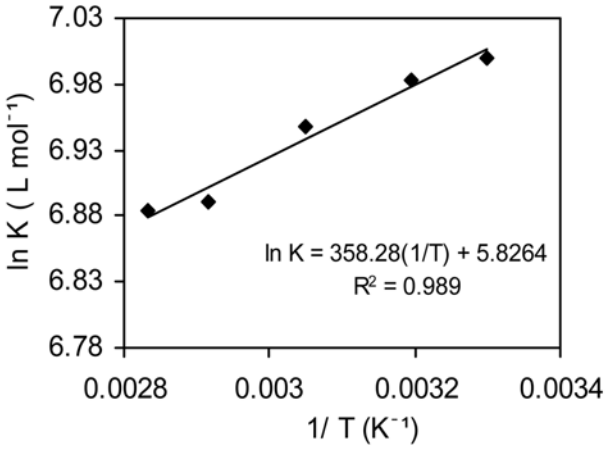

Fig. 8. Plot of ln K versus 1/T.

Where 55.5 is the concentration of water in solution (mol L^{-1}) replaced by the studied inhibitor. The enthalpy and entropy of adsorption (ΔH_{ads} and ΔS_{ads}) can be calculated by using Eq. (15),

$$\ln K = \ln\left(\frac{1}{55.5}\right) - \frac{\Delta G_{ads}}{RT};\ \Delta G_{ads} = \Delta H_{ads} - T\Delta S_{ads}$$
$$\ln K = \ln\left(\frac{1}{55.5}\right) - \frac{\Delta H_{ads}}{RT} + \frac{\Delta S_{ads}}{R} \tag{15}$$

Fig. 8 represents the plot of ln K versus 1/T. The obtained line represents a slope of ($-\Delta H_{ads}/R$) and an intercept of [ln(1/55.5)+ $\Delta S_{ads}/R$]. The values of K, ΔG_{ads}, ΔH_{ads} and ΔS_{ads} are listed in Table 4. The large negative values of ΔG_{ads} ensure the spontaneity of the adsorption process and the stability of the adsorbed layer on the low carbon steel surface. Generally, values of $-\Delta G_{ads}$ around 20 kJ mol^{-1} or lower are consistent with electrostatic interaction between the charged molecules and the charged metal (physisorption), those around 40 kJ mol^{-1} or higher involve charge sharing or transfer from organic molecules to the metal surface to form a coordinate type of bond (chemisorption) [17,18]. On the other hand, Bayoumi and Ghanem [19] reported that the adsorption of naphthalene disulphonic on the

Table 4. Thermodynamic parameters for adsorption of 2-HBTA on low carbon steel in industrial water at different temperatures and at 1.44 m s^{-1}

T (K)	R^2	K (L mol^{-1})	ΔG_{ads} (kJ mol^{-1})	ΔH_{ads} (kJ mol^{-1})	ΔS_{ads} (J mol^{-1} K^{-1})
303	0.989	1,096	−27.75		
313	0.989	1,078	−28.63	−2.98[a]	81.84[a]
328	0.982	1,040	−29.90		
343	0.997	896	−30.84	−2.96[b]	81.90[b]
353	0.983	976	−31.99		

[a]Values obtained from Eq. (15)
[b]Values obtained from Eq. (16)

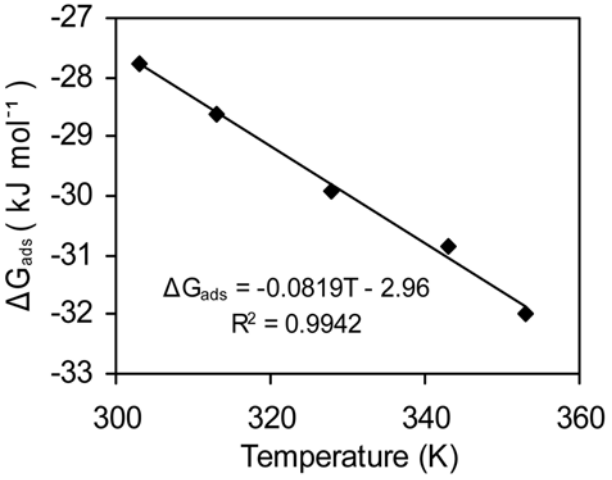

Fig. 9. Plot of ΔG_{ads} versus absolute temperature.

mild steel is chemisorption ($-\Delta G_{ads}$=28.47 kJ mol^{-1}). Thus, the obtained values of ΔG_{ads} here suggest that the chemisorption of 2-HBTA occurred onto the low carbon steel surface in industrial water. Moreover, the values of ΔH_{ads} and ΔS_{ads} also can be calculated by using the following equation:

$$\Delta G_{ads}=\Delta H_{ads}-T\Delta S_{ads} \quad (16)$$

Fig. 9 shows the plot of ΔG_{ads} versus T which gave a slope of $-\Delta S_{ads}$ and an intercept of ΔH_{ads}. The values obtained are in very good agreement with those obtained from plotting of Eq. (15), confirming the exothermic of adsorption process of 2-HBTA on low carbon steel surface in industrial water.

6. Adsorption Property of 2-HBTA

2-HBTA has two heteroatoms N and S in the thiazole ring. These heteroatoms have an ability to coordinate with transition metals such as iron and its alloys via the d-orbital of the metals and the empty p- or d-orbital of heteroatoms in the inhibitor molecules. Further, the sulfur atom is responsible for improving the inhibition efficiency of 2-HBTA on low carbon steel surface. This is due to the high electronegativity of S which acts by forming a stronger binding of the inhibitor molecules on the metal surface.

In addition the p-ë orbitals of benzene ring (aromaticity) can overlap with the d-orbital of the metal leading to bond formation.

With regards to 2-HBTA, the lone pair of electrons of "N" atom of hydrazine attached to the thiazole ring provides an additional anchoring site for the inhibitor to bind with the metal surface, thereby increasing the strength of adsorption and hence inhibition, as it has reported that N of NH_2 is involved in complexation [20].

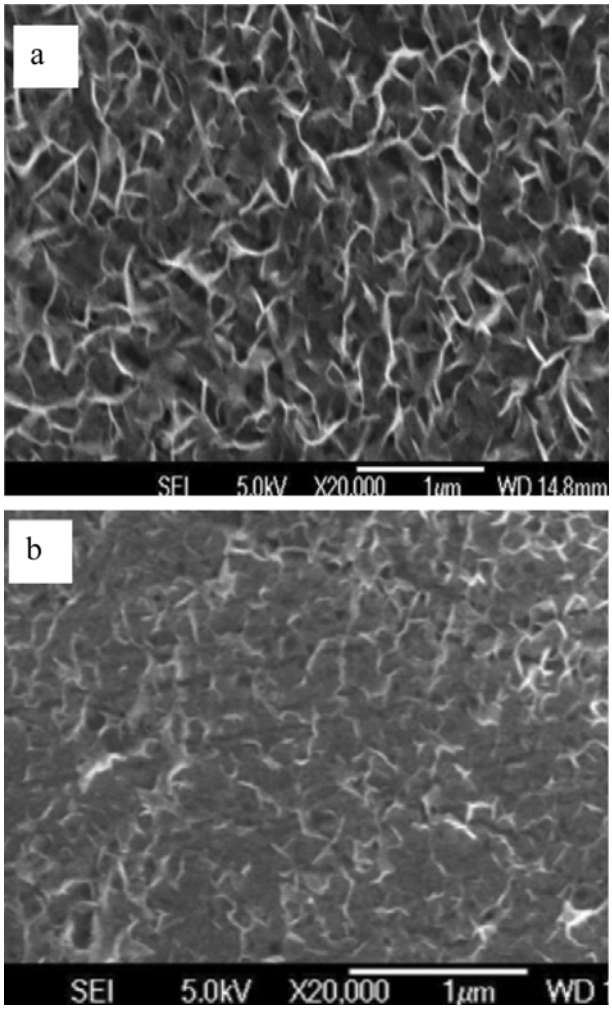

Fig. 10. SEM images of low carbon steel in industrial water solution after 10 hrs Immersion at 55 °C and at 1.56 m s^{-1}: (a) without inhibitor (b) with 4.2×10^{-3} M of 2-HBTA.

7. SEM Analyses

SEM analyses were conducted in order to characterize the protective layer that formed on the low carbon steel surface. SEM images in the uninhibited and inhibited solutions at 55 °C are presented in Fig. 10(a) and 10(b), respectively. After exposure of low carbon steel to uninhibited solution, the corroded surface appeared to dissolve uniformly with large cracks and deep terraces (Fig. 10(a)). In the presence of optimum concentration of 2-HBTA, the corroded surface showed small and smooth cracks (Fig. 10(b)), which are due to the complex film of Fe-2-HBTA formed on the surface, thereby offering better protection towards corrosion. After 10 hrs of immersion in the inhibited solution, the low carbon surface was partly covered with a layer containing the molecules of 2-HBTA. It can be concluded from this analysis that the molecules of 2-HBTA are incorporated in the surface of low carbon steel either as precipitate or, more likely, as a part of the protective layer.

Table 5. Box-Wilson statistical calculations of CR, real variables and error

Run No.	Coded variables			Real variables			$^{a}CR_{meas}$ (gmd)	$^{b}CR_{cal}$ (gmd)	e_i (gmd)
	X_1	X_2	X_3	X_1 (°C)	X_2 (m s^{-1})	X_3 (M)			
1	−1	−1	−1	40	1.56	1.37×10^{-3}	4.00	4.69	−0.69
2	1	−1	−1	70	1.56	1.37×10^{-3}	7.12	7.16	−0.04
3	−1	1	−1	40	1.90	1.37×10^{-3}	4.88	5.38	−0.50
4	1	1	−1	70	1.90	1.37×10^{-3}	7.94	7.94	0.00
5	−1	−1	1	40	1.56	3.45×10^{-3}	2.98	3.05	−0.07
6	1	−1	1	70	1.56	3.45×10^{-3}	5.70	5.27	0.43
7	−1	1	1	40	1.90	3.45×10^{-3}	2.98	3.01	−0.03
8	1	1	1	70	1.90	3.45×10^{-3}	5.89	5.29	0.60
9	−1.732	0	0	30	1.73	2.41×10^{-3}	3.96	3.28	0.68
10	1.732	0	0	80	1.73	2.41×10^{-3}	6.78	7.41	−0.63
11	0	−1.732	0	55	1.44	2.41×10^{-3}	4.72	4.40	0.32
12	0	1.732	0	55	2.02	2.41×10^{-3}	5.12	5.04	0.08
13	0	0	−1.732	55	1.73	6.09×10^{-4}	8.12	7.44	0.68
14	0	0	1.732	55	1.73	4.20×10^{-3}	3.01	3.75	−0.74
15	0	0	0	55	1.73	2.41×10^{-3}	5.12	5.19	−0.07

[a]CR obtained by experiments and [b]CR calculated by using Eq. (21)

APPLICATION OF BOX-WILSON STATISTICAL METHOD TO THE EXPERIMENTAL RESULTS

In general, the purpose of an experimental design is to find useful relationships between controllable variables and the observed response. The calculations were performed by using CR obtained from mass loss measurements. A second-order polynomial mathematical model is employed in the present work by using the following equation [21,22]:

$$CR = b_o + \sum_{i=1}^{p} b_i X_i + \sum_{i=1}^{p} b_{ii} X_i^2 + \sum_{i}^{p}\sum_{j}^{p} b_{ij} X_i X_j \quad (17)$$

The relationships between the coded variables and the corresponding real variables are as follows:

$$X_{Coded} = \frac{X_{Actual} - X_{Centre}}{X_{Centre} - X_{Minimum}} \times \sqrt{p} \quad (18)$$

Where X_{Actual} is X_1 (temperature in °C), X_2 (velocity in m s^{-1}) and X_3 (inhibitor concentration in M), $X_{Centre}=(X_{Min.}+X_{Max.})/2$ for the given ranges, and p is the number of variables. The number of experiments (N) was estimated as follows:

$$N = 2^p + 2p + 1 \quad (19)$$

Rewriting Eq. (17) for the three variables in the present work as follows:

$$CR = b_o + b_1x_1 + b_2x_2 + b_3x_3 + b_4x_1x_2 + b_5x_1x_3 + b_7x_1^2 + b_8x_2^2 + b_9x_3^2 \quad (20)$$

The design of the coded data has the properties that $\sum \frac{x_i}{N} = \sum \frac{x_i x_j}{N} = 0$ and $\sum \frac{x^2}{N} = 0.933$, then Eq. (20) was rearranged as follows:

$$B_o = b_o + 0.933\times b_7 + 0.933\times b_8 + 0.933\times b_9$$

By substituting b_o into Eq. (20) one obtains,

$$CR = B_o + b_1x_1 + b_2x_2 + b_3x_3 + b_4x_1x_2 + b_5x_1x_3 + b_6x_2x_3 + b_7(x_1^2 - 0.933) + b_8(x_2^2 - 0.933) + b_9(x_3^2 - 0.933) \quad (21)$$

$$b_i = \sum x_i \times (CR)_i / \sum x_i^2 \quad (22)$$

Values of CR calculated were obtained from Eq. (21) after substituting B_o and b_i. Table 5 shows real variables, CR calculated and error, which were conducted according to the Box-Wilson method and the experimental response was represented by the measured CR. The analysis of variance F-value was used for testing the significance of each effect in Eq. (21). The values of degrees of freedom (γ=N−10) and the experimental error variance ($S_r^2=\sum_{i}^{N} e_i^2/\gamma$) are 5 and 0.65, respectively. The estimated variance of coefficients ($S_b^2=S_r^2/\sum X_i^2$) was determined. The values are presented in Table 6. By using $F_{0.95}$, after substituting B_o and b_i values in Eq. (21) neglecting only the effect of X_1X_2 due to its under value, it can be rearranged as,

$$CR = 5.22 + 1.19X_1 + 0.184X_2 - 1.089X_3 - 0.069X_1X_3 - 0.189X_2X_3 + 0.049(X_1^2 - 0.933) - 0.159(X_2^2 - 0.933) + 0.14(X_3^2 - 0.933) \quad (23)$$

This equation represents the best form of mathematical model which correlates the CR to the three variables in terms of the coded variables. An equivalent in terms of actual variables would be more useful in the estimation of CR of low carbon steel in a solution of industrial water and 2-HBTA at any desired conditions. The following equation could be obtained for the present experimental design:

$$CR = -19.52 + 0.083T + 23.4V + 214.2C - 1088.2VC - 5.7V^2 + 129438C^2 \quad (24)$$

Where T is the temperature (°C), C is the inhibitor concentration (M) and V is the fluid velocity (m s^{-1}). The optimum combination of variables conditions was found by the first derivative for Eq. (23) for the dependent variables which was taken with respect to X_1, X_2 and X_3 as follows:

Table 6. Analysis of variance of variable effects

Effect	$\sum X_i^2$	$\sum CR_i \times X_i$	$b_i = \sum X_i \times CR_i / \sum X_i^2$		$S_b^2 = S_r^2 / \sum X_i^2$	F-value (b_i^2/S_b^2)	$F_{0.95}$=0.0661
X_0	15.0	78.321	B_o	5.221			
X_1	14.0	16.694	b_1	1.192	0.046	30.627	S
X_2	14.0	2.580	b_2	0.184	0.046	0.732	S
X_3	14.0	−15.241	b_3	−1.089	0.046	25.525	S
X_1X_2	8.0	0.130	b_4	0.016	0.081	0.003	NS
X_1X_3	8.0	−0.550	b_5	−0.069	0.081	0.058	NS
X_2X_3	8.0	−1.510	b_6	−0.189	0.081	0.438	S
U_1[a]	12.9	0.634	b_7	0.049	0.050	0.048	NS
U_2	12.9	−2.061	b_8	−0.159	0.050	0.505	S
U_3	12.9	1.804	b_9	0.140	0.050	0.387	S

[a]$U_i = X_i^2 - 0.933$, S: Significant; NS: Not Significant

$$\frac{\partial CR}{\partial X_1} = 0,\ \frac{\partial CR}{\partial X_2} = 0 \text{ and } \frac{\partial CR}{\partial X_3} = 0$$

The three equations obtained with three unknowns can be solved by using GWB 3.22-XP software. The real values were determined from Eq. (18). Therefore, the optimization values are 38.5 °C, 1.66 m s^{-1} and 3.69×10^{-3} M.

CONCLUSION

1. The optimum conditions obtained from polarization and mass loss measurements of the studied inhibitor on low carbon steel surface in industrial water are 4.2×10^{-3} M, 55 °C and 1.56 m s^{-1}; and 3.69×10^{-3} M, 38.5 °C and 1.66 m s^{-1} as they were obtained from the Box-Wilson statistical method.
2. The lower values of activation energy in presence of 2-HBTA than those in its absence and the higher negative values of Gibbs free energy indicated that the adsorption process of 2-HBTA on low carbon steel in industrial water is chemisorption.
3. The adsorption of 2-HBTA was found to obey the Langmuir adsorption isotherm, and the inhibition efficiency was temperature independent.
4. The corrosion current density (I_{corr}) in presence and in absence of inhibitor increased with increasing the velocity up to 1.56 m s^{-1}, and then it began decreasing. The adsorbed film containing the investigated compound was identified by SEM analysis.
5. The experimental results obtained were well correlated with the Box-Wilson statistical method.

ACKNOWLEDGMENTS

One of the authors (Badiea A. M.) thanks the Minister of Higher Education and the Ministry of Oil in the Yemen Republic for the financial support of this research and acknowledges the by University of Mysore and JCE Engineering, Mysore for providing research facilities.

REFERENCES

1. E. Cano, D. M. Bastidas, J. Simancas and J. M. Bastidas, *Corrosion*, **61**, 5 (2005).
2. J. M. Bastidas, J. De Damborenea and A. Vazquez, *J. Appl. Electrochem*, **27**, 345 (1997).
3. J. De Damborenea, J. M. Bastida and A. Vazquez, *Electrochim. Acta*, **42**, 455 (1997).
4. Horvath, Tibor, Eirka, Kutson, Gyogy and Adam, Magy. *Kem. Foly*, **98**, 363 (1997).
5. N. Jallerat, F. L. Port, F. Bourelier and Vu. K. Qng, *International Congress on Metallic Corrosion, Toronto, Canada*, **4**, 404 (1984).
6. W. Roberston and J. Electrochem., Soc., **98**, 94 (1951).
7. M. Bouklah, N. Benchat, B. Hammouti, A. Aouniti and S. Kertit, *Mater. Lett*., **60**, 1901 (2006).
8. A. Leng and M. Stratmann, *Corros. Sci*., **34**, 1657 (1993)
9. L. R. M. Estevao and R. S. V. Nascimento, *Corros. Sci*., **43**, 1133 (2001).
10. V. S. Sastry, *Corrosion inhibitors, principles and applications*, John Wiley & Sons, New York (1998).
11. G. Baril, C. Blanc, M. Keddam and N. Pebere, *J. Electrochem. Soc*., **151**, 488 (2003).
12. O. Benali, L. Larabi, M. Traisnel, L. Gengembre and Y. Harek, *Appl. Sur. Sci*., **253**, 6130 (2007).
13. B. G. Ateya, B. M. Abo Elkhai and I. A. Abdel Hamid, *Corros. Sci*., **16**, 163 (1976).
14. W. L. McCabe, C. S. Julian and P. Hariott, *Unit operations of chemical engineering*, 4th ed, McGraw Hill, p. 217, 219 and 690 (1985).
15. R. K. Sinnott, *Chemical engineering*, Vol. 1, 1st ed., Pergamon Press, Oxford (1983).
16. S. Bilgic and N. Caliskan, *Appl. Sur. Sci*., **152**, (1999).
17. F. M. Donahue and K. Nobe, *J. Electrochem. Soc*., **112**, 886 (1965).
18. E. Kamis, F. Bellucci, R. M. Latanision and E. S. H. El-Ashry, *Corrosion*, **47**, 677 (1991).
19. F. M. Bayoumi and W. A. Ghanem, *Mater. Lett*., **59**, 3806 (2005).
20. M. J. M. Campbell, R. Grazeskawiak and S. G. Juneja, *J. Inorg. Nucl. Chem*., **36**, 2485 (1974)
21. D. G. Montgomery, *Design and analysis of industrial experiments*, 3rd ed., New Delhi (1976).
22. G. E. P. Box and K. B. Wilson, *J. Royal Statis. Soc*., **1**, 13 (1951).